# Coherent Addressing of Individual Neutral Atoms in a 3D Optical Lattice

Yang Wang, Xianli Zhang, Theodore A. Corcovilos,[†] Aishwarya Kumar, and David S. Weiss[*]

*Physics Department, The Pennsylvania State University, 104 Davey Lab, University Park, Pennsylvania 16802, USA*

We demonstrate arbitrary coherent addressing of individual neutral atoms in a $5 \times 5 \times 5$ array formed by an optical lattice. Addressing is accomplished using rapidly reconfigurable crossed laser beams to selectively ac Stark shift target atoms, so that only target atoms are resonant with state-changing microwaves. The effect of these targeted single qubit gates on the quantum information stored in nontargeted atoms is smaller than $3 \times 10^{-3}$ in state fidelity. This is an important step along the path of converting the scalability promise of neutral atoms into reality.

Trapped neutral atoms possess the essential features of a qubit [1]: their internal states can be initialized and measured, they have long coherence times [2], and they can be entangled [3,4]. Since a useful quantum computer needs many qubits, the fact that thousands of neutral atoms can be optically trapped near each other gives them a strong head start over other qubit candidates in terms of scalability. Eigenstate flipping of individual atoms in one- and two-dimensional arrays have previously been demonstrated, but in situations with no nearby stored quantum information [5,6]. Coherent addressing of all the atoms in a sparsely populated plane of lattice sites has been demonstrated, in a way that does not affect atoms in the two adjacent planes [7]. A quantum computer requires the ability to arbitrarily change the quantum state of only targeted individual atoms. A high-fidelity single qubit gate on a target site in a 2D array of microtraps was recently demonstrated, but without nearby quantum information and with up to 9% state-flipping cross talk with adjacent atoms [8]. In this Letter, we demonstrate coherent addressing of targeted atoms in a $5 \times 5 \times 5$ 3D array with a minimal effect on nearby quantum information.

Scalable optical traps for individual neutral atoms include 2D optical lattices [9–12], arrays of dipole traps [13–15], and 3D optical lattices [16]. The optimal spacing of individual traps is a balance, on the one hand, between ready entanglement and high density, which favor closely spaced atoms, and on the other hand, independent addressability, which favors more widely spaced atoms. A similar trade-off exists for 3D versus 2D geometries, where scaling for entanglement, density, and error correction favor 3D, but addressability favors 2D. Whatever the geometry, nearby quantum information must remain unperturbed by the addressing light. We tackle this issue head on, with microwave addressing of individual atoms in a 3D lattice and ac Stark shifting addressing beams that pass directly through nontarget atoms. The methods we demonstrate here can be used to pursue higher densities in any geometry.

Our qubit states are the Cs $F = 3$ and 4 $m_F = 0$ hyperfine ground sublevels, which we call the storage basis. The

addressing scheme uses two circularly polarized addressing beams that cross at the target lattice site [see Fig. 1(a)], ac Stark shifting the target atom by approximately twice as much as any other atom [see Fig. 1(b)] [17–19]. We use the storage basis tune-out wavelength (880.250 nm) [20,21] for the addressing beams so the storage states experience minimal force from the addressing beams. The $m_F = 1$ (or $m_F = -1$) sublevels constitute the computational basis [22]. A first microwave pulse resonant with the target atom at $\omega_1$ coherently transfers the target atom to the computational basis while leaving all nontarget atoms in the storage basis. Then a second pulse at $\omega_2$ can arbitrarily change the target atom's quantum superposition in the computational basis. A third $\omega_1$ pulse then returns the target atom to the storage basis. As described below, a four-gate sequence for every two addressed qubits cancels the effects of addressing on nontarget atoms.
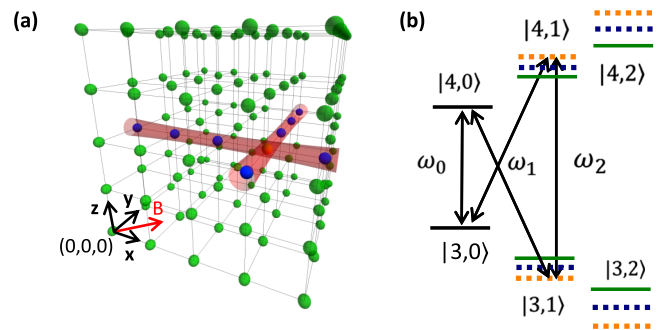


FIG. 1 (color online). (a) Diagram of addressing a $5 \times 5 \times 5$ array of neutral atoms. Each addressing beam can be parallel translated within 5 $\mu$s to any line of atoms, so that any site can be put at their intersection. The addressing beams are circularly polarized, and the 140 mG magnetic field is in the same plane. (b) The relevant part of the ground state energy level structure for addressing (not to scale). A target atom experiences twice the ac Stark shift of any other atom (its shift is illustrated by the orange dashed lines), so that, starting in the storage basis, $|3, 0\rangle$ and $|4, 0\rangle$ it alone is resonant with $\omega_1$. After it is transferred to the computation basis, $|3, 1\rangle$ and $|4, 1\rangle$, it alone is resonant with $\omega_2$.

Our experimental apparatus was largely described in Refs. [16,23]. A 3D optical lattice is made from three interfering pairs of blue-detuned (847.78 nm) laser beams, with 10° between the incident angles within a pair, and ~100 MHz frequency offsets between pairs, which creates a 200 $\mu$K deep, 4.9 $\mu$m spaced lattice in each direction with negligible tunneling. A random ~40% of the lattice sites in our target $5 \times 5 \times 5$ site array start with one atom, while the rest are empty [16]. We detect the occupancy of all lattice sites in a plane with negligible error by collecting the fluorescence from polarization gradient cooling with a 0.55 numerical aperture composite lens. By successively translating the lens along the optical axis, we make a 5 plane occupancy map (in 850 ms) without affecting the occupancy. The final atom hyperfine state is measured by clearing the $F = 4$ atoms with a resonant pulse, then making a new occupancy map. We cool the atoms in the $|F = 4, m_F = 4\rangle$ magnetic sublevel to near their vibrational ground state with projection sideband cooling [23]. We then use a series of five or six adiabatic rapid passage microwave pulses [23] to transfer them to the $|3, 0\rangle$ or $|4, 0\rangle$ state with 97.2% efficiency, where the loss is due to atoms that are left in high vibrational states after cooling, an issue that can likely be avoided with the use of higher lattice power [24]. After transfer, we adiabatically halve the lattice trapping frequency to 7.5 kHz.

We have a plan for converting partial site filling into unity occupancy in a subvolume that requires some of the methods demonstrated here [17,18]. For now, we simply address on a site-selective basis, regardless of the presence of an atom there. The images and data we report are produced from multiple such implementations.

To address a target atom, we use two orthogonal, 2.7 $\mu$m waist circularly polarized laser beams with 26 $\mu$m Rayleigh ranges [see Fig. 1(a)]. The beams are each reflected from a pair of MEMS mirrors, whose angles can be controlled over 0.5 deg with a ~5 $\mu$s reset time [25]. Using a 5-element optical transfer system, the angles are converted into beam translations at the atoms with a 30 $\mu$m range [25]. A series of control systems maintains the stability of the addressing beams, which we align to the atoms using atomic signals [26].

Site-selective state transfer is illustrated in Fig. 2. We point the addressing beams to the first target site and then turn on the light adiabatically (in 290 $\mu$s). We apply a 300 $\mu$s long microwave $\pi$ pulse, whose frequency we scan across the range that includes the $|4, 0\rangle$ to $|3, -1\rangle$ resonance for all atoms. We then adiabatically turn off the addressing light, move the MEMS mirrors, and repeat the process, sequentially targeting two lattice sites in each of two planes. Fig. 2(a) plots $R$, the ratio of the number of detected $F = 3$ atoms to the initial number of atoms. The green points are the signal from atoms that are never in the line of an addressing beam. The blue points are from atoms that are shifted by only one addressing beam. The orange points correspond to the signals from targeted sites. Figure 2(b) shows the summed atom pictures of the two planes with
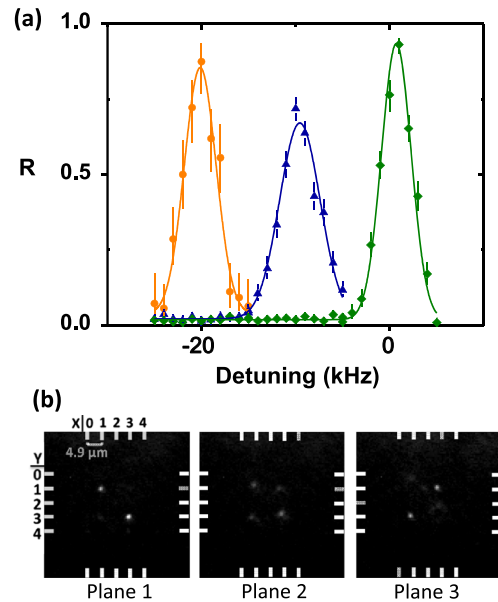


FIG. 2 (color online).   (a) Probability that an atom makes a transition from $|4, 0\rangle$ to $|3, -1\rangle$ as a function of the detuning of $\omega_1$ from the unshifted resonance. The orange points correspond to the four target sites in two planes addressed in this sequence, the blue points correspond to nontarget atoms traversed by addressing beams, and the green points correspond to all the other atoms. The solid lines are fits to Gaussians. The error bars are from counting noise. (b) Summed images of the raw signals from three planes using the value of $\omega_1$ that yields the orange peak in (a). Two sites in each of planes 1 and 3 are addressed in each implementation [labeled by (1, 1, 1), (3, 3, 1), (1, 3, 3), and (3, 1, 3)]. The signal in plane 2 is the out-of-focus light from the adjacent planes; out-of-focus atom images have nearly double the radius, the probability of them giving a false positive in our occupancy maps is below $10^{-6}$.

addressed atoms and the plane in between, taken at the target frequency at the orange peak in Fig. 2(a). The background 1.7% ± 0.4% of nontarget atoms in the $F = 3$ state are unrelated to the microwave transfer, but rather due to lattice spontaneous emission, and imperfections in the clearing process and the transfer from the $|4, 4\rangle$ state.

Figure 3 illustrates coherence in these lattices with data on the clock transition without addressing beams. We start with the atoms in the $|3, 0\rangle$ state, apply a microwave $\pi/2$ pulse, wait for a time $T/2$, apply a $\pi$ pulse, wait for another $T/2$, and then apply a final $\pi/2$ pulse with a scanned phase. We plot the contrast of the resulting fringe as a function of $T$, with insets showing representative fringes. The echo is needed mostly because of imperfect sideband cooling, which leaves from 25% to 40% of the atoms in higher vibrational levels with different lattice light differential ac Stark shifts (130 Hz/vibrational level); $T_2^*$ is 26 ms for the central $3 \times 3 \times 3$ core and 10 ms overall. The coherence time ($T_2'$) exceeds 7 s, limited by lattice spontaneous emission. The coherence time significantly exceeds those of other single atom neutral atom experiments because
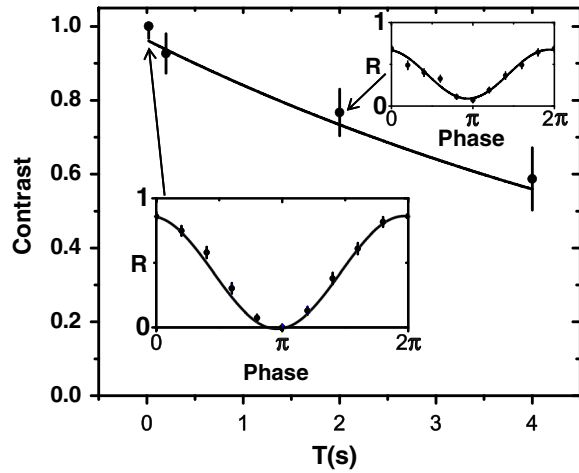
FIG. 3 (color online).   Fringe contrast for a spin-echo sequence
on all the atoms. The fit exponential time constant is 7.4 s. Since
the contrast is lost due to spontaneous emission, the rate of which
depends on an atom's vibrational state, the true function is more
complicated. The insets are the unnormalized fringes at the
indicated times, where the phase of the final $\pi/2$ pulse in
$\pi/2$-$\pi$-$\pi/2$ is varied.

these atoms are vibrationally cold in all directions, which
minimizes inhomogeneous broadening and spontaneous
emission [3,4,7]. Coherence times for storing light with
trapped atoms of 16 s have been achieved using a "magic"
magnetic field [27]; while perhaps applicable here, such
large fields would come at the expense of the robustness of
our storage basis. There is up to a 10% loss of atoms in the
detected signal (visible in the Fig. 3 insets), 3% from
imperfect transfer, and 7% from a ~15 s collision rate with
background gas atoms. Improved vacuum and more lattice
power to improve and speed up the projection cooling
should ultimately bring losses below 1%.

To demonstrate coherent addressing, we first use a $\pi/2$
pulse (100 $\mu$s at $\omega_0$) to put all the atoms into the super-
position $(|3,0\rangle + |4,0\rangle)/\sqrt{2}$. We then execute the address-
ing procedure discussed above. By empirically adjusting
the microwave polarization, we equalize the $|3,0\rangle$ to $|4,1\rangle$
and $|4,0\rangle$ to $|3,1\rangle$ Rabi frequencies, so the transfer to and
from the computational basis can be made with a simple $\pi$
pulse. We generate the three microwave frequencies with a
single direct digital synthesizer. The phase of the $\omega_2$ pulse
can be adjusted so that it rotates the Bloch vector about any
axis in the **X**-**Y** plane, and its amplitude can be adjusted to
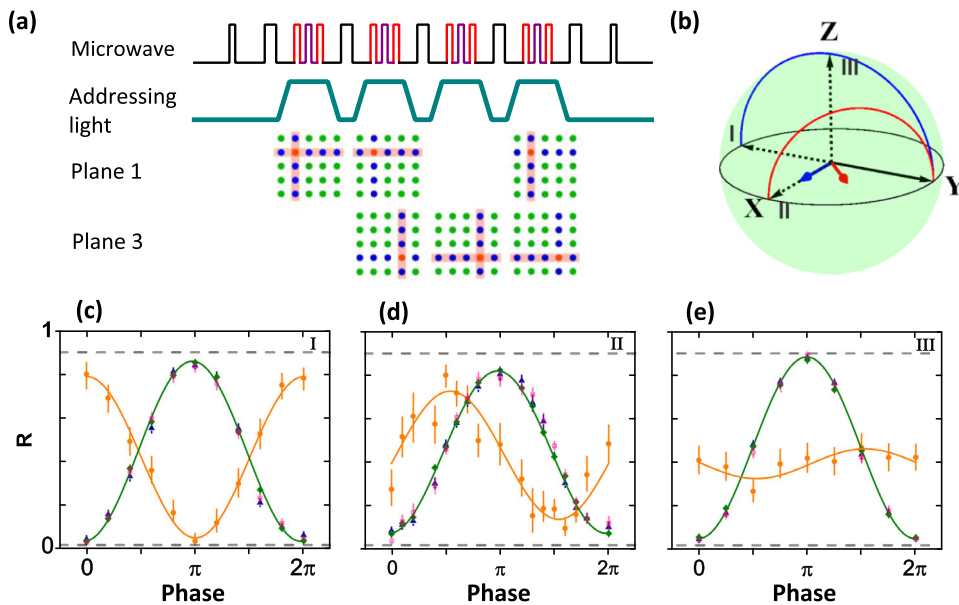give any rotation angle [for example, see Fig. 4(b)]. Thus,



FIG. 4 (color online).   Arbitrary single qubit gates. (a) The addressing pulse sequence. The top row shows the timing of the microwave
pulses, which have Blackman temporal profiles. Black corresponds to $\omega_0$, red to $\omega_1$, and purple to $\omega_2$. The timing gaps are enhanced for
clarity. The second row shows the addressing beam pulses versus time, and the third and fourth rows show the corresponding addressing
beam locations. The atom color scheme is that of Fig. 1. The second and fourth sets of pulses are "dummy" gates—they have no target
atom. Their purpose is to cancel out the phase shifts on nontarget atoms. (b) A Bloch sphere representation of qubit rotations due to the
$\omega_2$ pulses. The solid black arrow is the initial quantum state, the blue and red arrows correspond to torque vectors, the red and blue arcs
are the Bloch vector paths during the gates, and the dashed black arrows are the final states, labeled I, II, and III. (c) Interference fringe
due to gate I of Fig. 4(b). The orange circles are due to the four target atoms, the blue triangles are for line atoms, the pink squares are for
nearest neighbors, and the green diamonds are for other atoms. The gate target is a $\pi$-shifted fringe. (d) Interference fringe due gate II of
Fig. 4(b). The gate target is a $\pi/2$-shifted fringe. (e) Interference fringe due to gate III of Fig. 4(b). The gate target is a horizontal line of
half the peak of the unaffected fringe.

arbitrary rotations on a Bloch sphere can be made. A final $\omega_0$ $\pi/2$ pulse with scanned phase then probes the quantum states of all the atoms.

We have demonstrated single qubit gates on two non-coplanar target atoms, with MEMS mirrors redirection during the sequence. Each application of an addressing beam results in a $\sim 0.35\pi$ phase shift for the nontarget atoms on its line, and the microwave pulses cause $0.1\pi$ scale off-resonant ac Zeeman phase shifts on nontarget atoms. To cancel these unwanted shifts, we use "dummy" gates to ensure that each nontarget atom experiences each of these shifts twice, with its state flipped between the two times, as illustrated by the pulse sequence in Fig. 4(a). The orange circles in Fig. 4(c) show results for a $\pi$ rotation (in 150 $\mu$s) about the **X** axis (gate I), in Fig. 4(d) a $\pi$ rotation about the $(\mathbf{X} + \mathbf{Y})/\sqrt{2}$ axis (gate II), and in Fig. 4(e) a $\pi/2$ rotation (in 75 $\mu$s) about the **X** axis (gate III). The green diamonds in Figs. 4(c)–4(e) show interference fringes for nontarget atoms that see no addressing light, the blue triangles for nontarget atoms that are in line with addressing beams, and the pink squares for the 6 atoms adjacent to each target atom.

The spin-echo-type approach that we employ on non-target atoms only imperfectly cancels unwanted shifts for the target atoms, since the phase shifts experienced by a target atom during the dummy pulses differ from those during the targeting pulse. Accordingly, we empirically cancel the shifts due to the dummy pulses when adjusting the phase of the $\omega_2$ pulse for each gate. Eventually it will be necessary to model all dummy shifts to predetermine their effect on the gates.

The fringes of Figs. 4(c)–4(e) provide basic information about gate fidelity, allowing us to project the Bloch vector of an atom before the final $\pi/2$ pulse onto its target Bloch vector [26]. The spin-echo infrastructure compromises the (identity gate) fidelity of nontarget atoms by 0.01 to 0.02, depending on how carefully the pulse parameters have been adjusted. The addressing light and microwaves cause a marginal change in identity gate fidelity of $-0.001 \pm 0.003$ and $+0.002 \pm 0.003$ for the line atoms and nearest neighbors, respectively; that is, even the most vulnerable non-target atoms are unaffected at the level of 0.003. The fidelity of the gates on the target atoms themselves (including the spin echo errors) are 0.95, 0.91, and 0.93 for the gates in Figs. 4(c)–4(e), respectively. Gate I has higher quality because the two coherent halves of the atom spend the same time in all sublevels. Gate fidelities can ultimately be improved, perhaps to levels obtained in similar systems without site addressing [28,29], by varying the spin-echo pulse phases [30], better projection cooling, better $B$-field stability, more tightly locked addressing beam positions, better addressing beam spatial modes, and quantum control techniques [31].

In conclusion, we have demonstrated arbitrary single qubit gates on targeted atoms in a 125 atom 3D array. Given the 7 s coherence time and the $\sim 1$ ms total time for each single qubit gate, we can in principle perform thousands of such gates before significant decoherence occurs. Deeper, farther detuned lattices will ultimately allow for superior and faster initial cooling, as well as faster gates. The next steps on the road to a quantum computer in this system will be to fill in vacancies and implement entangling Rydberg gates in this already highly scaled system.

*Corresponding author.
dsweiss@phys.psu.edu
†Present address: Department of Physics, Duquesne University, 600 Forbes Avenue, 317 Fisher Hall, Pittsburgh, PA 15282, USA.

[1] D. P. DiVincenzo, Fortschr. Phys. **48**, 771 (2000).
[2] I. Bloch, Nature (London) **453**, 1016 (2008).
[3] T. Wilk, A. Gaetan, C. Evellin, J. Wolters, Y. Miroshnychenko, P. Grangier, and A. Browaeys, Phys. Rev. Lett. **104**, 010502 (2010).
[4] L. Isenhower, E. Urban, X. L. Zhang, A. T. Gill, T. Henage, T. A. Johnson, T. G. Walker, and M. Saffman, Phys. Rev. Lett. **104**, 010503 (2010).
[5] C. Weitenberg, M. Endres, J. F. Sherson, M. Cheneau, P. Schauss, T. Fukuhara, I. Bloch, and S. Kuhr, Nature (London) **471**, 319 (2011).
[6] D. Schrader, I. Dotsenko, M. Khudaverdyan, Y. Miroshnychenko, A. Rauschenbeutel, and D. Meschede, Phys. Rev. Lett. **93**, 150501 (2004).
[7] J. H. Lee, E. Montano, I. H. Deutsch, and P. S. Jessen, Nat. Commun. **4**, 2027 (2013).
[8] T. Xia, M. Lichtman, K. Maller, A. W. Carr, M. J. Piotrowicz, L. Isenhower, and M. Saffman, Phys. Rev. Lett. **114**, 100503 (2015).
[9] W. S. Bakr, J. I. Gillen, A. Peng, S. Folling, and M. Greiner, Nature (London) **462**, 74 (2009).
[10] J. F. Sherson, C. Weitenberg, M. Endres, M. Cheneau, I. Bloch, and S. Kuhr, Nature (London) **467**, 68 (2010).
[11] L. W. Cheuk, M. A. Nichols, M. Okan, T. Gersdorf, V. V. Ramasesh, W. S. Bakr, T. Lompe, and M. W. Zwierlein, Phys. Rev. Lett. **114**, 193001 (2015).
[12] M. Miranda, R. Inoue, Y. Okuyama, A. Nakamoto, and M. Kozuma, Phys. Rev. A **91**, 063414 (2015).
[13] C. Knoernschild, X. L. Zhang, L. Isenhower, A. T. Gill, F. P. Lu, M. Saffman, and J. Kim, Appl. Phys. Lett. **97**, 134101 (2010).
[14] M. J. Piotrowicz, M. Lichtman, K. Maller, G. Li, S. Zhang, L. Isenhower, and M. Saffman, Phys. Rev. A **88**, 013420 (2013).
[15] F. Nogrette, H. Labuhn, S. Ravets, D. Barredo, L. Béguin, A. Vernier, T. Lahaye, and A. Browaeys, Phys. Rev. X **4**, 021034 (2014).
[16] K. D. Nelson, X. Li, and D. S. Weiss, Nat. Phys. **3**, 556 (2007).
[17] D. S. Weiss, J. Vala, A. V. Thapliyal, S. Myrgren, U. Vazirani, and K. B. Whaley, Phys. Rev. A **70**, 040302(R) (2004).

[18] J. Vala, A. V. Thapliyal, S. Myrgren, U. Vazirani, D. S. Weiss, and K. B. Whaley, Phys. Rev. A **71**, 032324 (2005).

[19] C. Zhang, S. L. Rolston, and S. Das Sarma, Phys. Rev. A **74**, 042316 (2006).

[20] L. J. LeBlanc and J. H. Thywissen, Phys. Rev. A **75**, 053612 (2007).

[21] B. Arora, M. S. Safronova, and C. W. Clark, Phys. Rev. A **84**, 043401 (2011).

[22] It is also possible to use the $|3, 1\rangle$ and $|4, -1\rangle$ states for storage, and our storage states for computation, since both manifolds are first-order $B$-field insensitive, but that choice would require slowing down our gates by about an order of magnitude. N. Lundblad, J. M. Obrecht, I. B. Spielman, and J. V. Porto, Nat. Phys. **5**, 575 (2009).

[23] X. Li, T. A. Corcovilos, Y. Wang, and D. S. Weiss, Phys. Rev. Lett. **108**, 103001 (2012).

[24] B. J. Lester, A. M. Kaufman, and C. A. Regal, Phys. Rev. A **90**, 011804 (2014).

[25] C. Knoernschild, C. Kim, F. P. Lu, and J. Kim, Opt. Express **17**, 7233 (2009).

[26] See Supplemental Material at http://link.aps.org/supplemental/10.1103/PhysRevLett.115.043003 for a discussion of stabilization and alignment procedures and for fidelity calculations.

[27] Y. O. Dudin, L. Li, and A. Kuzmich, Phys. Rev. A **87**, 031801 (2013).

[28] K. R. Brown, A. C. Wilson, Y. Colombe, C. Ospelkaus, A. M. Meier, E. Knill, D. Leibfried, and D. J. Wineland, Phys. Rev. A **84**, 030303 (2011).

[29] S. Olmschenk, R. Chicireanu, K. D. Nelson, and J. V. Porto, New J. Phys. **12**, 113007 (2010).

[30] P. Callaghan, *Principles of Nuclear Magnetic Resonance Microscopy* (Oxford University Press, New York, 1993).

[31] A. Smith, B. E. Anderson, H. Sosa-Martinez, C. A. Riofrio, I. H. Deutsch, and P. S. Jessen, Phys. Rev. Lett. **111**, 170502 (2013).